Springer

KSME

Journal of Mechanical Science and Technology 32 (8) (2018) 3537~3545
www.springerlink.com/content/1738-494x(Print)/1976-3824(Online)
DOI 10.1007/s12206-018-0704-9

Calculation of time dependent mesh stiffness of helical planetary gear system using analytical approach †

Mohsen Rezaei, Mehrdad Poursina*, Shahram Hadian Jazi and Farhad Haji Aboutalebi

Department of Mechanical Engineering, Faculty of Engineering, University of Isfahan, Isfahan, 81744-73441, Iran

(Manuscript Received October 14, 2017; Revised December 19, 2017; Accepted April 18, 2018)

Abstract

Time-dependent mesh stiffness is a most important reason of vibration and dynamic excitation in gear sets. In this research, analytical formulas of the helical gear set and the planetary gear system are combined to calculate the time-dependent mesh stiffness of the helical planetary gear system. For this purpose, at the first step, the analytical equations are derived for the spur gear pair. Then by dividing a helical tooth into the several independent thin spur tooth slices, the helical gear pair mesh stiffness is extracted. Finally, these equations are extended to the helical planetary gear system. The suggested analytical results and those which obtained by the finite element method (FEM) are compared and are in good agreement when the helix angle is less than 15 degrees. Also, the helical planetary gear system mesh stiffness in different cases such as fixed carrier, fixed sun gear and fixed ring gears is calculated. These results show that the value of mesh frequency ratio in each case scales the mesh stiffness shapes in the rotation angle direction. In other words, mesh frequency ratio parameter determines the number of meshing period in each rotation of planets.

Keywords: Helical gears; Planetary; Mesh stiffness; Analytical; Finite element method

1. Introduction

Planetary gear systems are generally used in precise and sensitive applications in industries due to their compaction and high torque transmission ability at low weight [1]. Time-dependent mesh stiffness in planetary gear system reveals the variation in the stiffness because of the change in the number of tooth pairs in contact and change in their contact positions.

Finite element, experimental and analytical approaches were generally used to calculate the gears mesh stiffness by previous researchers.

Wang and Howard estimated the spur gear set stiffness using the FEM [2]. Liang et al. [3] have proposed three new models in the FEM for the evaluation of standard involute spur gear mesh stiffness. They compared the results of their new proposed models with the existing models. Also, the FEM is used to model the systems and to evaluate the results obtained from analytical models in Refs. [4-8].

The major difficulty of the FEM is taking much time. If the FEM is used to evaluate the series of gear pairs mesh stiffness, each condition has to be modeled and it is difficult to express the effect of changes in results due to changes in system parameters. Also, the FEM results are so dependent on mesh density and the kinds of elements.

Pandya and Parey [9] and Raghuwanshi and Parey [10] investigated the spur gears mesh stiffness using photoelasticity technique. They used stress intensity factor and energy release rate on the stress contours in the gear bodies to obtain the gears' mesh stiffness.

Yang and Lin [11] offered potential energy method to compute the mesh stiffness suitably and excellently. In this method, the relative contribution of different components, such as shear, bending and Hertzian contact stiffness, considered separately [12].

Yang and Lin [13] estimated the external– external spur gear mesh stiffness by the potential energy method. They considered axial, bending and Hertzian energy corresponding to axial, bending and Hertzian contact stiffness respectively.

Sainsot et al. [14] studied the gear body deflection and obtained an equation to determine the gear body stiffness due to the force between gears that applied to the gear tooth. Most researchers use their equation to import the effect of gear body deflection on the gear pair mesh stiffness.

Wan et al. [15] estimated the helical gear pair mesh stiffness by the method that they denominate to accumulated integral potential energy. They considered the helical tooth such as the series of independent spur teeth with the small width. They validate their results with finite element method. Marques et al. [16] have also proposed a different process to calculate the

*Corresponding author. Tel.: +98 3137934516, Fax.: +98 3137932746
E-mail address: Poursina@eng.ui.ac.ir
† Recommended by Associate Editor Sungsoo Na

load sharing and mesh stiffness of spur and helical gear pairs analytically.

Liang et al. [17] studied the spur planetary gear system and obtained the external-external and internal-external spur gear pairs mesh stiffness using the potential energy method.

On the other hand, dynamic models of some helical and double helical planetary systems have been studied by researchers. Eritenel and Parker [18] studied the modal properties of a helical planetary gear system in the three-dimensional formulation. They used constant values for sun-planet and ring-planet translational and tilting mesh stiffness in their study. Khoozani et al. [19] have also used constant mesh stiffness in their research.

Prashant and Kahraman [20, 21] have studied the dynamic modeling of the double-helical planetary gear system. They used time-invariant dynamic model at first and then investigated the influence of gyroscopic and time-varying mesh stiffness effects on it. They considered the time-varying mesh stiffness as constant values and cosine Fourier series form whose amplitudes and phase angles are obtained from static transmission error.

Mbarek et al. [22] studied the effects of load and meshing stiffness variation on modal properties of spur planetary gear system. They used spur sun-planet and ring-planet time-varying mesh stiffness in their model.

By studying the available literature in this field, it is observed that prior studies generally focused on the mesh stiffness calculation of one stage spur and helical gear pairs and spur planetary gear systems and there is no research directed on the analytical calculation of the helical planetary gear system mesh stiffness. Moreover, the studies on dynamic modeling of the helical planetary gear system focused on constant or approximate mesh stiffness values.

In this research, at first, analytical calculation of spur gear mesh stiffness and mesh stiffness attainment of the helical gear from the spur gear is explained. Then, the meshing of external-external and internal-external gear pairs is described. The mesh stiffness of each pair in the helical planetary gear system is obtained using the relations between the mesh stiffness of each pair in the planetary gear system. The results of the proposed method are validated by the FEM results. Then, the results of single stiffness and mesh stiffness of the helical sun-planet and ring-planet gear pairs are illustrated. Finally, the mesh stiffness of each pair in the helical planetary system in three cases, including fixed carrier, fixed ring gear, and fixed sun gear is demonstrated.

2. Analytical calculation of mesh stiffness

In this section, analytical calculation of helical planetary gear system mesh stiffness is described using a combination of helical and planetary exist theories of mesh stiffness calculation.

According to the potential energy method [23] the spur gear tooth is considered as a beam and then axial, bending and shear stiffness of that beam can be calculated analytically. Also the gear body as that beam foundation has a stiffness known as fillet-foundation stiffness, then the spur gear mesh stiffness is analytically computed by considering nine parts; axial, bending, shear and fillet-foundation stiffness for each gear and Hertzian stiffness of their contact [15, 24]. A beam model of a single tooth is shown in Fig. 1.

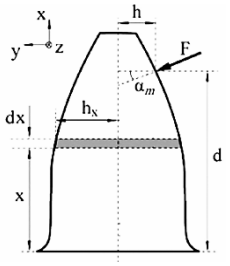

Fig. 1. A single tooth parameters.

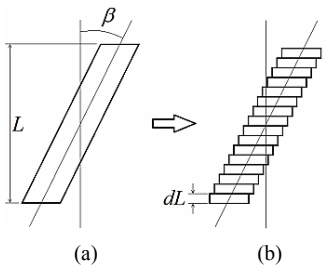

Fig. 2. (a) Helical tooth; (b) sliced thin spur teeth.

In the helical gears pair the contact zone started from zero length at the time that teeth come into contact and then gradually increase to a maximum and then decrease to zero at the end of their contact. This type of entering and leaving the contact of the helical gears causes different vibration characteristics with respect to the spur gears. Also, the calculation of the helical gears mesh stiffness isn't like that of the spur gears.

Nevertheless, when the helical tooth as Fig. 2(a) is divided into several independent thin slices with thickness dL as Fig. 2(b), helical tooth can be considered as several consecutive spur teeth that came in contact one after one with a certain rotational distance that can be computed with respect to the tooth helix angle and the number of slices. Also, the slices are considered with no connections between them which are negligible for the gears with thin faces and low helix angles [25].

The helical gear stiffness can be obtained by summing stiffness of all spur gear slices as Fig. 3. If the helical tooth slices are very few, the curve of the helical tooth stiffness against rotation angle isn't smooth. To solve this problem, the number of slices must be increased enough, Fig. 3(b).

2.1 External- external gear pair meshing

In the planetary gear set, sun-planet gear pair meshing is an example of external-external gear pair meshing which is shown in Fig. 4. In sun and planet gears the most important parameters such as root radius, r_d, freedom radius, r_f, and

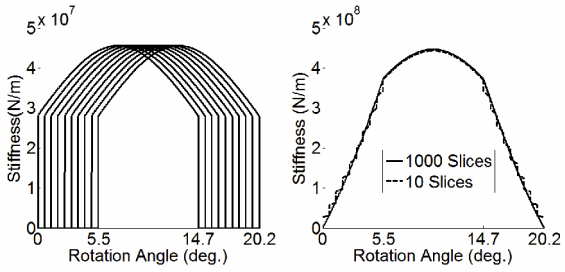

(a) (b)

Fig. 3. (a) Stiffness of thin spur gear teeth; (b) stiffness of helical gear tooth calculated by summation of thin spur gear teeth stiffness.

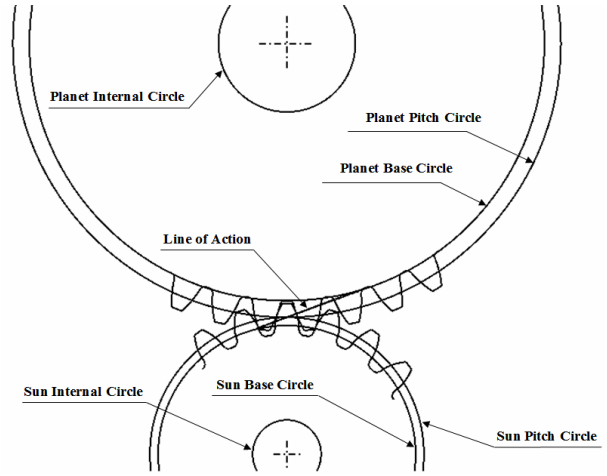

Fig. 4. The meshing of sun- planet pairs.

addendum radius, r_a, are calculated from Eqs. (1)-(3), respectively.

$$r_d = r - \left(h_a^* + c^*\right)m \tag{1}$$

$$r_f = r - h_a^* m \tag{2}$$

$$r_a = r + h_a^* m \tag{3}$$

where r, h_a^* and C^* are the pitch radius, the addendum coefficient and the tip clearance coefficient, respectively.

As shown in Fig. 1, the coordinates of any point on the involute region are given by Eqs. (4) and (5) [26]:

$$x\left(\alpha_m\right) = r_b\left[\left(\alpha_m + \theta_b\right)\sin\left(\alpha_m\right) + \cos\left(\alpha_m\right)\right] \tag{4}$$

$$h\left(\alpha_m\right) = r_b\left[\left(\alpha_m + \theta_b\right)\cos\left(\alpha_m\right) - \sin\left(\alpha_m\right)\right] \tag{5}$$

where r_b is the base radius that is calculated in all kind of gears by $r_b = r\cos\left(\alpha\right)$ and α is pressure angle of gear, α_m is the variable angle of the contact force in each point with respect to the root circle of gear, and θ_b is the half angle of a tooth measured on the base circle, which is calculated from Eq. (6):

$$\theta_b = \frac{\pi}{2N} + inv\left(\alpha\right) \tag{6}$$

where $inv\left(\alpha\right)$ is the involute function of the pressure angle, α which is calculated by Eq. (7):

$$inv\left(\alpha\right) = \tan\left(\alpha\right) - \alpha\,. \tag{7}$$

For modeling of the sun and planet teeth, it is important to find the angles that show the start point and the end point of the tooth involute profile and meshing. As it is known, the involute curve starts from the gear base circle and ended at the addendum, but when the base radius is smaller than the root radius, the involute curve starts from the root circle and the angle that involute curve starts, α_0 satisfied Eq. (8). When the base radius is greater than the root radius, α_0 is equal to zero.

$$r_b\left[\left(\alpha_0 + \theta_b\right)\sin\left(\alpha_0\right) + \cos\left(\alpha_0\right)\right] - r_d = 0\,. \tag{8}$$

It is clear that the meshing path of each tooth is from the freedom circle to the addendum, and related angle that meshing is started, α_1, satisfied Eq. (9). But if the base radius is bigger than the freedom radius, meshing starts from the base circle and. α_1 is equal to zero.

$$r_b\left[\left(\alpha_1 + \theta_b\right)\sin\left(\alpha_1\right) + \cos\left(\alpha_1\right)\right] - r_f = 0\,. \tag{9}$$

Also, the angle that the meshing and the involute curve are ended, α_2 satisfied Eq. (10):

$$r_b\left[\left(\alpha_2 + \theta_b\right)\sin\left(\alpha_2\right) + \cos\left(\alpha_2\right)\right] - r_a = 0\,. \tag{10}$$

Numerical methods such as Bisection method can be used to obtain three angles α_0, α_1 and α_2.

2.2 Internal-external gear pair meshing

In Planetary gear system, the meshing of the ring and the planet gears is an example of external-internal gear pair meshing that is shown in Fig. 5. In the ring gear some important parameters such as the root radius, r_d, the freedom radius, r_f, and the addendum radius, r_a, are calculated from Eqs. (11)-(13):

$$r_d = r + \left(h_a^* + c^*\right)m \tag{11}$$

$$r_f = r + h_a^* m \tag{12}$$

$$r_a = r - h_a^* m\,. \tag{13}$$

The coordinates of any point on the involute region of the ring gear are given by Eqs. (14) and (15):

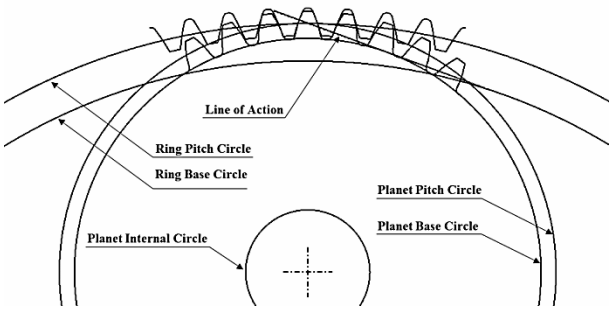

Fig. 5. The meshing of ring- planet pairs.

$$x(\alpha_m) = r_b\left[(\alpha_m + \theta_b)\sin(\alpha_m) + \cos(\alpha_m)\right] \quad (14)$$

$$h(\alpha_m) = \left[r_b\left[(\alpha_m + \theta_b)\cos(\alpha_m) - \sin(\alpha_m)\right] - 2h_p\right]. \quad (15)$$

In which α_m is the variable angle of the contact force at each point with respect to the root circle of the tooth and h_p is the half of tooth thickness on the pitch circle which is calculated from Eq. (16):

$$h_p = r_b\left[(\alpha_p + \theta_b)\cos(\alpha_p) - \sin(\alpha_p)\right] \quad (16)$$

where α_p is the perpendicular line angle on the involute curve at the pitch point, which satisfies Eq. (17):

$$r_b\left[(\alpha_p + \theta_b)\sin(\alpha_p) + \cos(\alpha_p)\right] - r = 0. \quad (17)$$

To model the ring teeth, it is important to find the angles that show the start and the end point of the tooth involute profile and the meshing of gears. As it is known the involute curve starts from the base circle and ended at the root of the tooth in the internal gears. While the teeth number of the ring gear is greater than 42, the involute curve starts from the root circle because of the smaller amount of the base radius. In this situation the angle that the involute curve and the meshing are started, α_2 is given by Eq. (18):

$$r_b\left[(\alpha_2 + \theta_b)\sin(\alpha_2) + \cos(\alpha_2)\right] - r_a = 0. \quad (18)$$

When the base radius is smaller than the freedom radius, the meshing length of the tooth starts from the freedom circle and continues to the addendum circle. In the end of contact angle, α_1 can be calculated from Eq. (19):

$$r_b\left[(\alpha_1 + \theta_b)\sin(\alpha_1) + \cos(\alpha_1)\right] - r_f = 0. \quad (19)$$

Also, the end angle of the involute curve, α_0, is obtained by Eq. (20):

$$r_b\left[(\alpha_0 + \theta_b)\sin(\alpha_0) + \cos(\alpha_0)\right] - r_d = 0. \quad (20)$$

2.3 Planetary gear system mesh stiffness

A planetary gear system contains a sun gear, a ring gear, a carrier that one of them has to be fixed and two others can connect to input and output shafts, and several planets gears that rotate between the sun and ring gear. There are three cases in the planetary system include fixed carrier, fixed sun gear, and fixed ring gear. When the carrier is fixed, all meshing between sun, ring, and planets in the system are considered as they actually are as gear pairs with immobile centers. Then the mesh stiffness of each pair, in this case, is equal to that of fixed center gears. Also in the planetary gear system, at the same time, there are in the number of planets, sun-planet and ring-planet pairs that are in meshing. The mesh stiffness of each planet with the sun or ring gear is the same, but with a phase difference [27].

There is no difference between the meshing regions of each pair of gears in the planetary gear system, whether the carrier is fixed or rotating. That means shapes and values of the mesh stiffness of each case are the same. The only thing that changed in each case is the mesh period. In fixed sun gear and fixed ring gear cases a parameter λ is defined as mesh frequency ratio to scale the mesh stiffness by multiplying in planet gear rotation angle [17].

3. Results validation by FEM

The power transmission of the gear systems is due to the rotation and the meshing of the gear teeth. ABAQUS commercial software is used for the finite element simulation of the helical planetary gear system to obtain the mesh stiffness. In quasi-static FE models, a torque will be applied to the planet gear to run the model. This torque makes the planet to rotate and makes contact with fixed gear (sun or ring). For modeling sun, planet and ring gear, 52600, 69000 and 63300 tetrahedral elements with the quadratic order are used respectively. From ABAQUS results, the angular displacement caused by this input torque is obtained. Eq. (21) is given the torsional stiffness of the gear, K_T, at a specific position [28].

$$K_T = \frac{T_i}{\theta} \quad (21)$$

where T_i is the applied torque to pinion and θ is the angular displacement of the pinion.

Linear gear mesh stiffness, K_L, expressed the coupling between torsional and transverse motions in the system. Linear mesh stiffness calculated from the torsional mesh stiffness with the relationship shown in Eq. (22).

$$K_L = \frac{K_T}{R_p^2}. \quad (22)$$

In Eq. (22) R_p is the pitch radius of pinion.

Now, in order to validate the analytical results, the linear mesh stiffness that obtained from FE simulation is compared

Table 1. Helical planetary gear system parameters.

Parameter	Value
Normal module (mm)	1
Normal pressure angle (deg.)	20
Helix angle (deg.)	15
Teeth number of planet gears	16
Teeth number of sun gear	16
Teeth number of ring gear	48
Shaft radius of planets (mm)	2
Shaft radius of sun (mm)	2
Face width (mm)	5
Module of elasticity (GPa)	207
Poison ratio	0.3

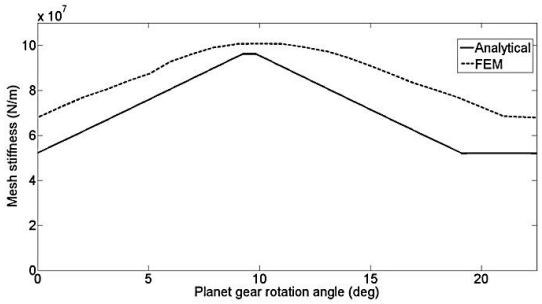

Fig. 6. AM and FEM results of helical sun-planet mesh stiffness.

with analytical results. Gear system parameters that are used to model the system in FE software and the analytical method, are presented in Table 1.

3.1 Results of external-external gear pair

In this section, at first, a pair of external- external helical gear is modeled in ABAQUS software. Then by changing the position of the gears in different situation of mesh, the angular displacement of the pinion gear caused by input torque at the pitch point is extracted. Finally, according to Eqs. (21) and (22) the single stiffness of the helical gear pair is calculated at the desired position of the mesh. This process is started from the beginning of contact and continues to the end of the contact of the gear pair.

Comparison of two methods for sun-planet mesh stiffness is shown in Fig. 6. As it is shown in Fig. 6, the trend of the analytical and FE results are similar and in good agreement. The difference between the two methods is acceptable. These differences are due to limitations that should be considered in the selection of the mesh size. Because, in the FE model with a very small size of the elements, the computational time is increased significantly.

3.2 Results of external-internal gear pair

Comparison of analytical and the FEM mesh stiffness results of the ring-planet pair that shown in Fig. 7 illustrated that the trend of analytical and the FEM results are similar and the results are on the same scale. Also, the difference between the two methods is in an acceptable range. As mentioned before, this difference is due to the limitation of the selection in the size of the element in the FEM method. In addition, the stiffness of the outer body of the ring gear in the analytical method is ignored.

Table 2. Parameters of helical planetary gear system.

Parameter	Value
Normal module (mm)	2
Normal pressure angle (deg.)	20
Helix angle (deg.)	15
Teeth number of planet gears	40
Teeth number of sun gear	20
Teeth number of ring gear	100
Number of planet	3
Shaft radius of planets (mm)	10
Shaft radius of sun (mm)	5
Face width (mm)	30
Module of elasticity (GPa)	207
Poison ratio	0.3
Pinion rotation direction	CCW

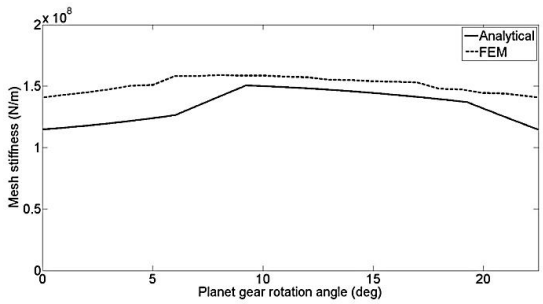

Fig. 7. AM and FEM results of helical ring-planet mesh stiffness.

4. Results and discussion

The results of this research are presented in four subsections. Planetary system parameters which are used for calculation and obtain results are presented in Table 2.

4.1 Single stiffness and mesh stiffness of helical sun-planet and ring-planet pair

Single tooth stiffness of the helical sun-planet gear pair is shown in Fig. 8. In the helical gear pairs the contact length starts from zero at the beginning of contact and then gradually increases to a maximum value, remains constant for a while and then slowly decreases to zero. Therefore, the single tooth mesh stiffness in helical gears has started from zero at the point (A) and increases until the point (B). Has a constant

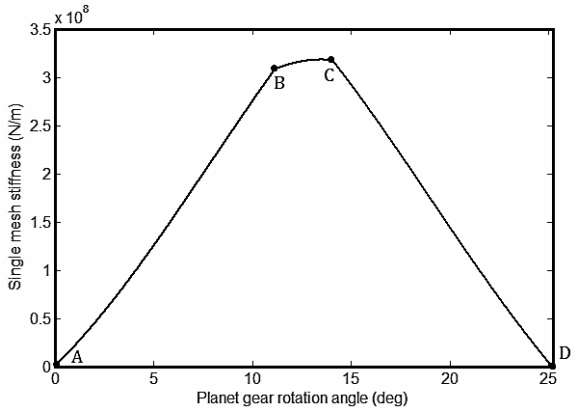

Fig. 8. Single tooth stiffness of helical sun-planet gear pair.

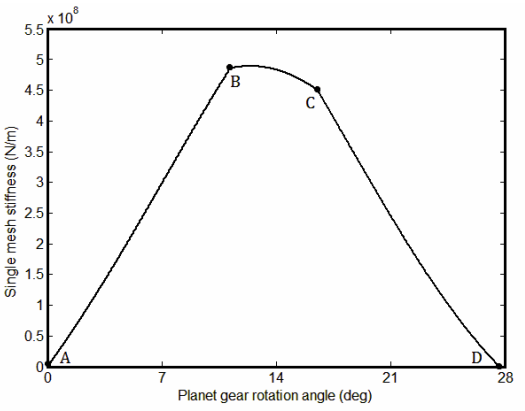

Fig. 10. Single tooth stiffness of helical ring-planet gear pair.

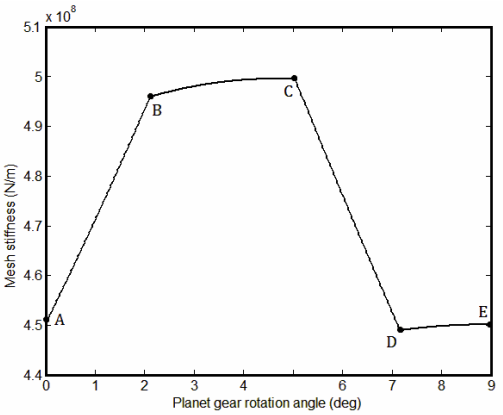

Fig. 9. A mesh cycle of helical sun-planet gear pair mesh stiffness.

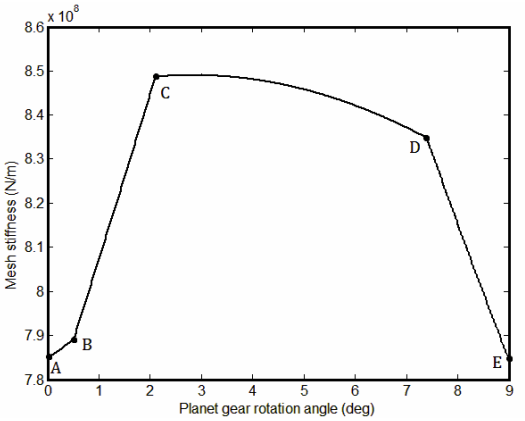

Fig. 11. A mesh cycle of helical ring-planet gear pair mesh stiffness.

contact length between the points (B) and (C). Then the value of the single mesh stiffness decreases from the point (C) to the point (D) because of reduction in the contact length.

Fig. 9 shows a mesh cycle of the helical sun-planet pair mesh stiffness. In this figure, the region from the point (B) to the point (C) represents two or more pair of teeth meshing, while the area from the point (D) to the point (E) represents a pair of teeth meshing.

Single tooth stiffness of the helical ring-planet pair is shown in Fig. 10. Similar to the Fig. 8, in this state also contact of two helical teeth started from zero at the point (A) and continues to complete contact in whole tooth width at the point (B). Has a constant contact length between the points (B) and (C). Then their contact is started to decrease at the point (C) and ended at the point (D).

A mesh cycle of helical ring-planet pair mesh stiffness is illustrated in Fig. 11. Often more than a pair of teeth is in contact in ring-planet gears meshing, because of the high contact ratio of this kind of gears pair. Therefore, the area from the point (C) to the point (D) represents the meshing of three or more pair of teeth, while the area from the point (A) to the point (B) represents the meshing of two pairs of teeth as can be seen in this figure.

4.2 Helical sun-planet and ring-planet gear pair mesh stiffness in the case of fixed carrier

Figs. 12 and 13 show the helical sun- planet and ring- planet gear pairs mesh stiffness in the half rotation of the planet gear when the carrier is fixed, respectively. As it is shown in Table 3, the planet gear has 40 teeth, then in half rotation of the planet gear, each of sun- planet and ring- planet gears pairs survive 20 mesh period. The point A′ in Figs. 12(a) and 13(a) corresponds to the initial meshing point of sun- planet and ring- planet gear pairs. The starting points for $k_{sp2,3}$ in Figs. 12(b) and (c) and $k_{rp2,3}$ in Figs. 13(b) and (c) are dissimilar due to the phase differences between the second and third pairs relative to the first pair.

4.3 Helical sun-planet and ring-planet gear pair mesh stiffness in the case of fixed ring gear

Figs. 14 and 15 show the helical sun- planet and ring- planet gear pairs mesh stiffness in half rotation of the planet gear in the case of fixed ring gear, respectively. In the case of fixed ring gear, sun- planet and ring- planet gear pairs will survive $20 \times \lambda_r$ (Approximately 16.6) mesh period in the half rotation

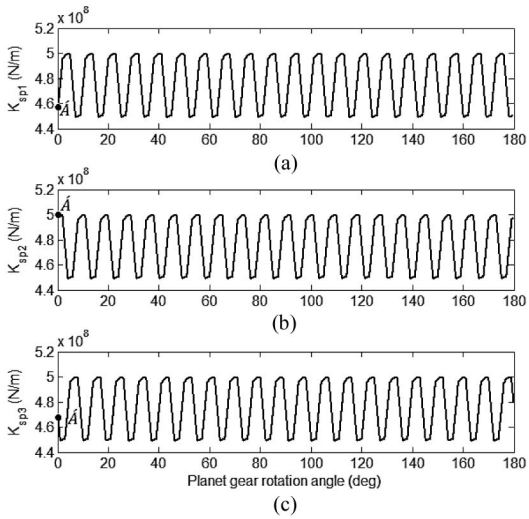

Fig. 12. Helical sun- planet gears mesh stiffness - fixed carrier: (a) First pair; (b) second pair; (c) third pair.

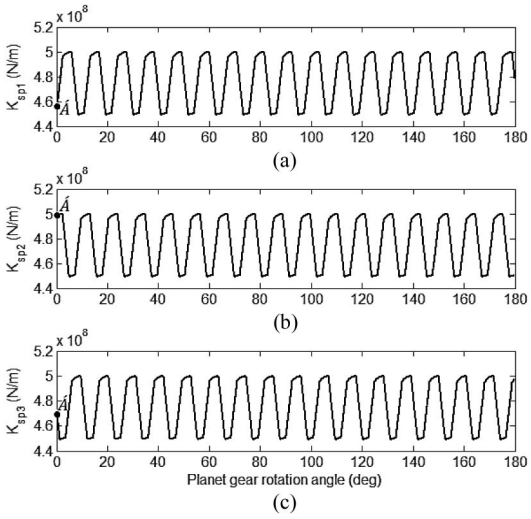

Fig. 14. Helical sun- planet gears mesh stiffness - fixed ring gear: (a) First pair; (b) second pair; (c) third pair.

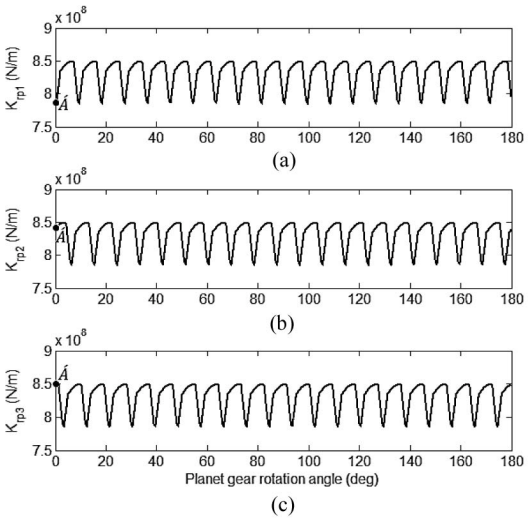

Fig. 13. Helical ring- planet gears mesh stiffness - fixed carrier: (a) First pair; (b) second pair; (c) third pair.

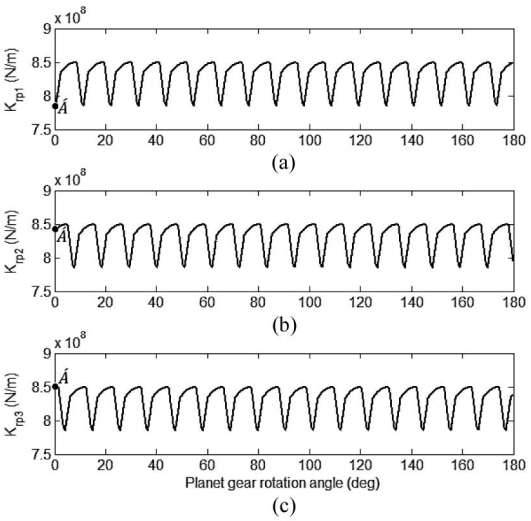

Fig. 15. Helical ring- planet gears mesh stiffness - fixed ring gear: (a) First pair; (b) second pair; (c) third pair.

of the planet gear. Similar to the fixed carrier case, change in the starting point A′ for $k_{sp2,3}$ and $k_{rp2,3}$ are due to phase differences between the second and the third pairs relative to the first pair.

4.4 Helical sun-planet and ring-planet gear pair mesh stiffness in the case of fixed sun gear

Figs. 16 and 17 show the helical sun- planet and ring- planet gear pairs mesh stiffness in half rotation of planet gear in the case of fixed sun gear, respectively. As in this case the sun gear is fixed, in half rotation of planet gear, each gear pair will experience $20\times\lambda_s$ (approximately 3.3) times tooth meshing. Similar to the fixed carrier and the fixed ring gear states, change in the starting point A′ for $k_{sp2,3}$ and $k_{rp2,3}$ are due to the phase differences between the second and the third pairs relative to the first pair.

5. Conclusion

In this research, analytical formulas of the helical gear and the planetary gear system mesh stiffness are combined to calculate the time-dependent mesh stiffness of the helical planetary gear system. For this purpose, at first step, the analytical equations were derived for the spur gear pair. Then by dividing the helical tooth into the several independent thin spur tooth slices, the helical gear pair mesh stiffness was extracted. Finally, these equations were extended to the helical planetary gear system. Results obtained from the analytical model for a sample of helical planetary gear system are compared with FEM results to validate the analytical method. Comparison of results shows that, when the helix angle is low, usually less

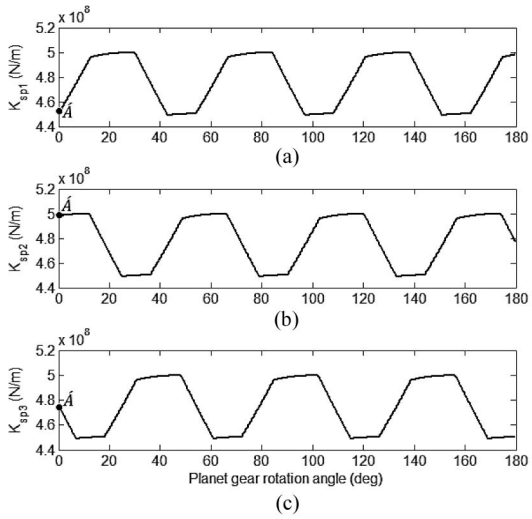

Fig. 16. Helical sun- planet gears mesh stiffness - fixed sun gear: (a) First pair; (b) second pair; (c) third pair.

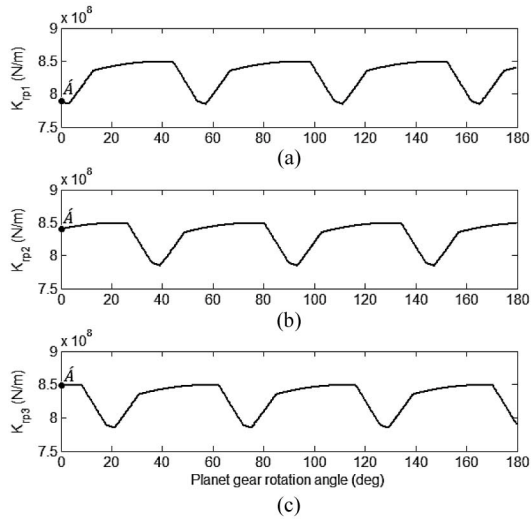

Fig. 17. Helical ring- planet gears mesh stiffness - fixed sun gear: (a) First pair; (b) second pair; (c) third pair.

than 15 degrees, dividing helical teeth to the series of spur teeth and using the potential energy method to calculate mesh stiffness in external and internal gears such as those used in planetary gear systems produce fairly correct results. Also, the helical planetary gear system mesh stiffness in different cases such as fixed carrier, fixed sun gear and fixed ring gears is calculated. These results show that the value of mesh frequency ratio in each case scales the mesh stiffness shapes in the rotation angle direction. In the other word, mesh frequency ratio parameter determines the number of meshing period in each rotation of planets.

This method can be used to calculate the mesh stiffness of a helical planetary system directly in dynamic modeling and simulations, instead of using constant or approximate values, and also for modeling tooth crack or spall in helical planetary gear systems.

References

[1] F. Chaari, W. Baccar, M. S. Abbes and M. Haddar, Effect of spalling or tooth breakage on gear mesh stiffness and dynamic response of a one-stage spur gear transmission, *European Journal of Mechanics-A/Solids,* 27 (4) (2008) 691-705.

[2] J. Wang and I. Howard, The torsional stiffness of involute spur gears, *Proceedings of the Institution of Mechanical Engineers, Part C: Journal of Mechanical Engineering Science,* 218 (1) (2004) 131-142.

[3] X. Liang, H. Zhang, M. J. Zuo and Y. Qin, Three new models for evaluation of standard involute spur gear mesh stiffness, *Mechanical Systems and Signal Processing,* 101 (2018) 424-434.

[4] H. Ma, R. Song, X. Pang and B. Wen, Time-varying mesh stiffness calculation of cracked spur gears, *Engineering Failure Analysis,* 44 (2014) 179-194.

[5] L. Chang, G. Liu and L. Wu, A robust model for determining the mesh stiffness of cylindrical gears, *Mechanism and Machine Theory,* 87 (2015) 93-114.

[6] X. Gu, P. Velex, P. Sainsot and J. Bruyère, Analytical investigations on the mesh stiffness function of solid spur and helical gears, *Journal of Mechanical Design,* 137 (6) (2015) 063301.

[7] H. Ma, X. Pang, R. Feng, J. Zeng and B. Wen, Improved time-varying mesh stiffness model of cracked spur gears, *Engineering Failure Analysis,* 55 (2015) 271-287.

[8] L. Cui, J. Huang, H. Zhai and F. Zhang, Research on the meshing stiffness and vibration response of fault gears under an angle-changing crack based on the universal equation of gear profile, *Mechanism and Machine Theory,* 105 (2016) 554-567.

[9] Y. Pandya and A. Parey, Experimental investigation of spur gear tooth mesh stiffness in the presence of crack using photoelasticity technique, *Engineering Failure Analysis,* 34 (2013) 488-500.

[10] N. K. Raghuwanshi and A. Parey, Experimental measurement of gear mesh stiffness of cracked spur gear by strain gauge technique, *Measurement,* 86 (2016) 266-275.

[11] D. C. H. Yang and J. Y. Lin, Hertzian damping, tooth friction and bending elasticity in gear impact dynamics, *Journal of Mechanisms, Transmissions, and Automation in Design,* 109 (2) (1987) 189-196.

[12] J. Meagher, X. Wu, D. Kong and C. H. Lee, A comparison of gear mesh stiffness modeling strategies, *Structural Dynamics*, 3 (2011) 255-263.

[13] D. C. H. Yang and J. Y. Lin, Hertzian damping, tooth friction and bending elasticity in gear impact dynamics, *Journal of Mechanisms, Transmissions, and Automation in Design,* 109 (2) (1987) 189-196.

[14] P. Sainsot, P. Velex and O. Duverger, Contribution of gear body to tooth deflections-A new bidimensional analytical formula, *Transactions-American Society of Mechanical Engineers Journal of Mechanical Design,* 126 (4) (2004) 748-752.

[15] Z. Wan, H. Cao, Y. Zi, W. He and Y. Chen, Mesh stiffness calculation using an accumulated integral potential energy method and dynamic analysis of helical gears, *Mechanism and Machine Theory,* 92 (2015) 447-463.

[16] P. Marques, R. Martins and J. Seabra, Analytical load sharing and mesh stiffness model for spur/helical and internal/external gears–Towards constant mesh stiffness gear design, *Mechanism and Machine Theory,* 113 (2017) 126-140.

[17] X. Liang, M. J. Zuo and T. H. Patel, Evaluating the time-varying mesh stiffness of a planetary gear set using the potential energy method, *Proceedings of the Institution of Mechanical Engineers, Part C: Journal of Mechanical Engineering Science,* 228 (3) (2014) 535-547.

[18] T. Eritenel and R. G. Parker, Modal properties of three-dimensional helical planetary gears, *Journal of Sound and Vibration,* 325 (1) (2009) 397-420.

[19] M. K. Khoozani, M. Poursina and A. P. Anaraki, Study of gyroscopic effects on the dynamics and vibrations of double-helical planetary gear set, *Proceedings of the Institution of Mechanical Engineers, Part K: Journal of Multi-body Dynamics* (2017) 1464419317725947.

[20] P. Sondkar, Dynamic modeling of double-helical planetary gear sets, *Ph.D. Dissertation*, The Ohio State University (2012).

[21] P. Sondkar and A. Kahraman, A dynamic model of a double-helical planetary gear set, *Mechanism and Machine Theory,* 70 (2013) 157-174.

[22] A. Mbarek, A. Hammami, A. F. D. Rincon, F. Chaari, F. V. Rueda and M. Haddar, Effect of load and meshing stiffness variation on modal properties of planetary gear, *Applied Acoustics* (2017).

[23] S. Wu, M. J. Zuo and A. Parey, Simulation of spur gear dynamics and estimation of fault growth, *Journal of Sound and Vibration,* 317 (3) (2008) 608-624.

[24] Q. Wang, Z. Li, H. Ma and B. Wen, Effects of different coupling models of a helical gear system on vibration characteristics, *Journal of Mechanical Science and Technology*, 31 (5) (2017) 2143-2154.

[25] L. Han, L. Xu and H. Qi, Influences of friction and mesh misalignment on time-varying mesh stiffness of helical gears, *Journal of Mechanical Science and Technology*, 31 (7) (2017) 3121-3130.

[26] H. Ma, R. Feng, X. Pang, R. Song and B. Wen, Effects of tooth crack on vibration responses of a profile shifted gear rotor system, *Journal of Mechanical Science and Technology*, 29 (10) (2015) 4093-4104.

[27] J. S. Kim, N. G. Park and H. W. Lee, Vibration analysis of a planetary gear system based on the transfer matrix method, *Journal of Mechanical Science and Technology*, 30 (2) (2016) 611-621.

[28] B. Fang, *CAE methods on vibration-based health monitoring of power transmission systems*, California Polytechnic State University (2013).

Mohsen Rezaei is a Ph.D. student of the Mechanical Engineering under supervision of Prof. M. Poursina since 2014, at the University of Isfahan, Isfahan, Iran. His research interests include the dynamics of gears, beam and plate theory and F.G.M. He received the B.Sc. and M.Sc. degrees in "Agricultural Machinery Engineering" from Shiraz University in 2010 and in "Mechanical Engineering" from Yasouj University in 2014, respectively.

M. Poursina is an Associate Professor of the Mechanical Engineering at the University of Isfahan, Isfahan, Iran. His research interests include the dynamics of gears, metal forming, machine design and optimization. He received the B.Sc., M.Sc. and Ph.D. degrees in mechanical engineering from Isfahan University of Technology, Isfahan, Iran in 1994, 1998 and 2003, respectively. During his Ph.D. he spent a sabbatical period at the Faculty of Engineering, University of Porto, Portugal.